ChemComm

COMMUNICATION

View Article Online
View Journal

Cite this: DOI: 10.1039/c5cc08002a

Received 25th September 2015,
Accepted 16th November 2015

DOI: 10.1039/c5cc08002a

www.rsc.org/chemcomm

Core–shell nano-FeS_2@N-doped graphene as an advanced cathode material for rechargeable Li-ion batteries†

Rui Tan,‡ Jinlong Yang,‡ Jiangtao Hu,‡ Kai Wang, Yan Zhao and Feng Pan*

We report the formation of core–shell nano-FeS_2@N-doped graphene as a novel cathode material and its mechanism for use in rechargeable Li-ion batteries. A benefit of the amount of FeS_2 nano-crystals as the core for Li-ion storage with high capacity and using coated N-doped graphene as the shell is that FeS_2@N-graphene exhibits a remarkable specific energy (950 W h kg^{-1} at 0.15 kW g^{-1}) and higher specific power (543 W h kg^{-1} at 2.79 kW g^{-1}) than commercial rechargeable LIB cathodes, as well as stable cycling performance (~600 W h kg^{-1} at 0.75 kW g^{-1} after 400 cycles).

Rechargeable Li-ion cells play a pivotal role in energy storage and electronic devices. However because the energy density of commercial cathode materials (including $LiCoO_2$, $LiNi_{0.5}Co_{0.2}Mn_{0.3}O_2$, $LiMn_2O_4$, $LiFePO_4$, *etc.*) for Li-ion batteries is approaching an upper limit, the next generation of cathodes need to be developed to satisfy the increased demand for advanced Li-ion cells.[1–4]

Among the advanced electrode materials based on metal sulfides,[5–8] pyrite FeS_2 is an interesting cathode material for a new type of Li-ion battery which has lots of advantages such as high theoretical capacity, good thermal stability, abundance in nature, being environmentally benign and its safety. By reaction with four Li-ions, pyrite FeS_2 can provide 890 mA h g^{-1} ($FeS_2 + 4Li^+ + 4e^- \rightarrow Fe + 2Li_2S$), which is about 5 times the specific capacity of $LiFePO_4$ (170 mA h g^{-1}). Based on the advantage of its remarkably high capacity for Li-ion storage, currently, pyrite FeS_2 has been widely utilized in commercial primary batteries and shows remarkable electrochemical performance.[9] Recently, pyrite FeS_2 has been investigated as secondary Li-ion cell cathodes or anodes.[10,11]

However, the main problems associated with FeS_2 being applied in rechargeable Li-ion cells include the polysulfide dissolution in electrolyte, low conductivity and large volume expansion. The mechanism of performance of pyrite FeS_2 is still a controversial subject. FeS_2, FeS_x and S have been reported to be the main products during the charge process,[12,13] of which Li_2S_x ($2 \leq x \leq 8$) may be formed during the charge–discharge procedure and can dissolve in the electrolyte leading to unfavorable side reactions with lithium metal. Owing to these reasons, the reported rechargeable cells that currently use FeS_2 have low coulombic efficiency and degrade quickly. In order to improve the performance of FeS_2 cells, numerous approaches have been tried, such as modifying the particle surface with conductive materials to enhance the electronic conductivity,[14,15] reducing the size and changing shape of the pyrite FeS_2 to shorten the Li-ionic transfer length,[16] utilizing all-solid-state electrolytes[17] and optimizing the polymer electrolyte[18–20] to prevent unfavorable shuttle effects of intermediate sulfur during operation. In previous studies, the cells with carbon-coated FeS_2 have shown good performance and long-term stability at high current rate, indicating that low cost carbon-coated pyrite FeS_2 is a promising candidate for commercial Li-ion batteries. For instance Yan Yu's group[21] developed a facile way to prepare FeS_2@porous C-nanooctahedra, which exhibit superior rate capability (at 5 C, 256 mA h g^{-1} obtained) and stable cycling performance (at 0.5 C, 495 mA h g^{-1} obtained after 50 cycles). Se-Hee Lee's group[22] used a polyacrylonitrile (PAN) matrix to modify the FeS_2 surface and to accommodate the volume expansion of FeS_2 during the charge–discharge procedure. Due to the low conductivity of the PAN matrix, the specific capacity of FeS_2@PAN is still low. A composite of FeS_2 microspheres@reduced graphene oxide was studied as a Li-ion cell anode by Chun-Sing Lee's group, which showed high capacity and long life performance.[11] They obtained 380 mA h g^{-1} at 10 C (8.9 A g^{-1}) over 2000 cycles. In addition, doping of heteroatoms (N, S, P, B, *etc.*) in the graphene shell[23–25] can improve its conductivity, which could be used to further optimize the electrochemical performance of pyrite FeS_2.

Herein, for the first time we report a facile and novel method to prepare pyrite nano-FeS_2 wrapped in an N-graphene framework (core–shell nano-FeS_2@N-graphene). The nano-size FeS_2 has a short Li-ionic diffusion distance, the N-graphene shell has optimized electronic conductivity to enhance structure stability, and the

School of Advanced Materials, Peking University, Peking University Shenzhen Graduate School, Shenzhen 518055, China. E-mail: panfeng@pkusz.edu.cn; Tel: +86-755-26033200

† Electronic supplementary information (ESI) available: Experimental procedures, theoretical details, figures and tables. See DOI: 10.1039/c5cc08002a

‡ These authors contributed equally to this work.

N-graphene framework between the nanoparticles possesses more fast charge transfer channels to reduce the resistance. As a result pyrite FeS_2 cells, LiTFSI/DOL/DME/$LiNO_3$, have superior electrochemical performance with a high reversible capacity of 484.7 mA h g^{-1} at 0.5 A g^{-1} corresponding to a specific capacity of 713.49 W h kg^{-1} and a fast rechargeable performance of 281.4 mA h g^{-1} (543 W h kg^{-1}) at 5 A g^{-1} at room temperature. Additionally, the cells with core–shell nano-FeS_2@N-graphene cathode have excellent long-term stability and high specific energy, containing 401.1 mA h g^{-1} (613.7 W h kg^{-1}) at 0.5 A g^{-1} after 400 cycles, which is higher than commercial rechargeable Li-ion batteries and also more stable than that of most other reported FeS_2 batteries.

The preparation scheme and basic characterisation of the as synthesized core–shell FeS_2@N-graphene are shown in Fig. 1 and 2. Fig. 1a briefly illustrates the synthesis process. In our previous work,[26] when Prussian blue precursors were calcined under an argon atmosphere, nano-Fe and Fe_xC were produced by reduction with glucose, and then carbon layers were attached to Fe_xC to generate a shell structure. When cooled down and exposed to air, core–shell γ-Fe_2O_3@N-graphene formed. Hereafter, core–shell γ-Fe_2O_3@N-graphene (SEM and TEM images seen in the Fig. S1, ESI†) was used as an important intermediate template to form core–shell FeS_2@N-graphene particles by sealing γ-Fe_2O_3@N-graphene and sulfur in a small tube and heating (see Fig. S2, ESI†). The tapped density of the obtained FeS_2@N-graphene is ~1.2 g cm^{-3}, comparable to commercial $LiFePO_4$.

To prove that the shell is N-doped graphene, element mapping is shown in Fig. 2c and Fig. S3 (ESI†). Nitrogen (pink) is combined with FeS_2 (blue and green). Considering the low nitrogen content and instrumental errors, XPS was carried out (Fig. 2d). The high resolution N1s XPS spectrum of FeS_2@N-graphene can be fitted to three main peaks (at 398.2, 400.2 and 401.3 eV). The peaks at low binding energy 398.2 and 400.2 eV correspond to pyridinic N and pyrrolic N respectively. The peak at high binding energy 400.8–401.3 eV means that carbon atoms within carbon layers are substituted by nitrogen atoms in form of graphic N.[27–30] The high resolution C_{1s} banding energy can be fitted to four components, corresponding to carbon atoms in five different chemical environments (Fig. S4c, ESI†): C_{sp^2} (284.49 eV), C_{sp^3} (285.2 eV), C–O (286.2 eV) and C═O (289.4 eV). The percentage of C_{sp^2} is 68.55, demonstrating that the carbon shell has a high degree of graphitization. In order to understand in more detail the graphene shell, shell materials were characterised by HRTEM (Fig. S4a, ESI†) and Raman spectroscopy (Fig. S4b, ESI†). A large number of graphene layers were observed in Fig. S4a (ESI†) and the 2D peak at 2700 cm^{-1} confirmed the graphene layer structure. Based on previously reported work,[23,24] N-doped graphene can further improve the conductivity and electrochemical performance of pyrite FeS_2. Meanwhile the thermal stability measured by thermogravimetric analysis (TG) seen in Fig. S5 (ESI†) shows that FeS_2@N-graphene is stable at high temperature (decomposition at ~300 °C).

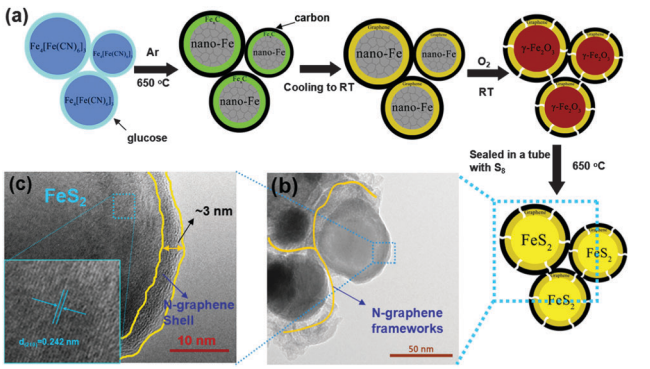

Fig. 1 (a) Brief illustration of the fabrication of FeS_2@N-graphene (RT: room temperature), (b) TEM image of FeS_2@N-graphene particles, (c) high-resolution TEM image of FeS_2@N-graphene particles.

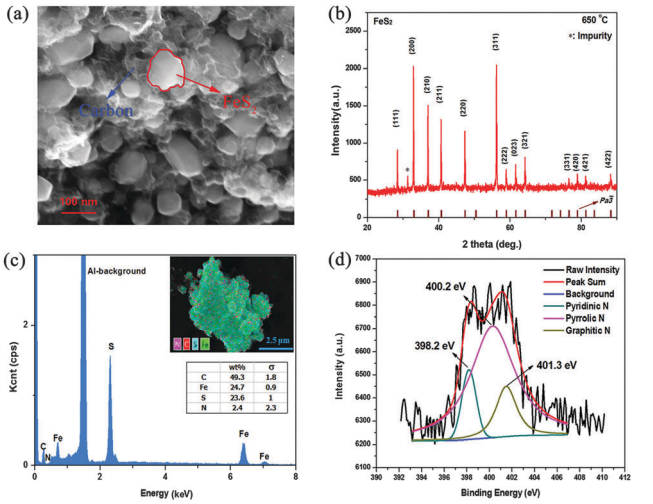

Fig. 2 (a) SEM image of FeS_2 particles (red) and carbon regions (blue), (b) XRD patterns, (c) EDX image (inserted SEM image and table show the element distribution and content of the sample respectively.), (d) binding energy of N1s in FeS_2@N-graphene sample.

The inserted SEM image in Fig. 2c shows that the core–shell nano-FeS_2@N-graphene composite aggregates as micron sized particles which share a boundary at the N-graphene layer. Li-ion electrode materials with micron dimensions can take advantage of high volumetric specific energies and facile processability for practical applications. As shown in Fig. 2a, the prime FeS_2 (red) particle, 50–100 nm in size, is closely wrapped by the N-doped graphene framework (blue). The XRD pattern (Fig. 2b) with well-defined diffraction peaks shows nano-FeS_2 with a cubic structure (JCPDF card no. 42-1340, space group $Pa\bar{3}$, a = 5.419 Å) without any other unwanted impurities like marcasite, greigite, pyrrhotite or sulfur. But because of utilizing glass tubes in the synthesis process, impurities inevitably occur in small amounts. The average particle size is approximately 50 nm as measured by XRD and calculated according to the Scherrer formula, which is correlated to the amount of prime FeS_2 nano-crystals in the core–shell measured by TEM in Fig. 2a.

In this structure, nano-sized FeS_2 has a short Li-ionic diffusion distance while the N-graphene frameworks with optimized electronic conductivity can supply more contact area to reduce resistance. This means that charge transfer channels are created around the particles. In order to obtain more detailed observations of the N-graphene frameworks connected to single prime FeS_2, the surface states of FeS_2 were investigated by TEM (Fig. 1b) and

HRTEM (Fig. 1c). Next to the N-graphene frameworks, the ~3 nm N-graphene shells are tightly attached to FeS_2. The advantage of the shell structure with excellent electronic conductivity is that it can both improve the conductivity of the FeS_2 surface as well as enhance the structural stability due to volume change in the charge–discharge process. Therefore, when combined with the advantages of short Li-ionic distance in the nano-size FeS_2, the structure stability enhancement by the N-graphene shell and the fast charge transfer paths around the N-graphene frameworks lead to the superior electrochemical performances of core–shell nano-FeS_2@N-graphene for Li-ion battery use.

The Li-ion storage performance of as-synthesis nano-FeS_2@N-graphene were studied by cyclic voltammetry (CV) and its electrochemical properties were studied using two-electrode coin cells. Fig. 3a shows the first four CV curves of nano-FeS_2@N-graphene with 1 M LiTFSI and 0.3 M $LiNO_3$ in DOL/DME at a scanning rate of 0.2 mV s^{-1}. For the first cycle, two wide reduction peaks (at approximately 1.48 and 1.22 V) and two oxidation reduction peaks (1.89 and 2.61 V) were seen. The reduction peaks at ~1.48 and 1.22 V are attributed to the decomposition of $LiNO_3$[31] (providing a large irreversible capacity), and the reduction of nano-FeS_2, which correspond to the voltage platform at the 1st cycle curve in Fig. S6 and S7 (ESI†).

As the cycle number increases, the redox reaction voltages are nearly unchanged, reflecting good reversibility of nano-FeS_2@N-graphene. The typical cycling curves in Fig. 3b and 4b show that the capacity of the cells decays very slowly with ~0.9 mA h g^{-1} per cycle from the 2nd to the 400th cycle at 0.5 A g^{-1}.

Combining with the CV analysis and XRD patterns at different charge/discharge state (Fig. S8), the reversible reaction mechanism and phase transformation were illustrated in Fig. 3c and d with the phase structure *vs.* electrochemical performance during the charge–discharge process with different "State" (State 1–4). During the discharging procedure (Fig. 3c and d), FeS_y ($y \leq 2$, State 3) transforms to Li_2FeS_2 (State 2) and then to Fe and Li_2S (State 1), from which Fe can form a conductive framework to promote the

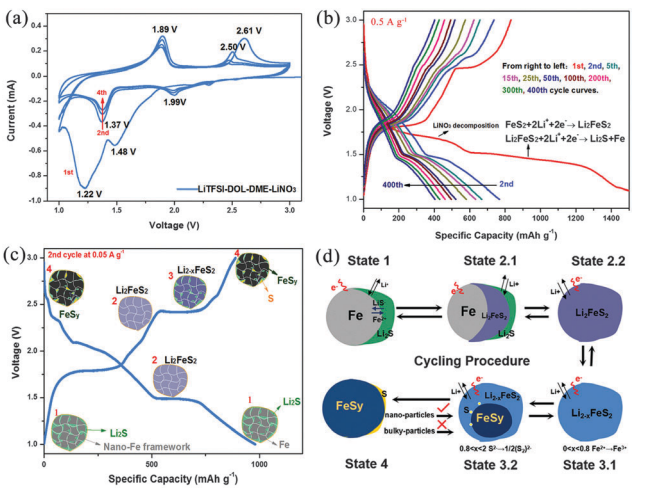

Fig. 3 (a) Cyclic voltammetry curves (from 1st to 4th cycle at 0.2 mV s^{-1}), (b) cycling curves from 2nd to 100th cycle at 0.5 A g^{-1}, (c and d) schematic diagram for reaction mechanism.

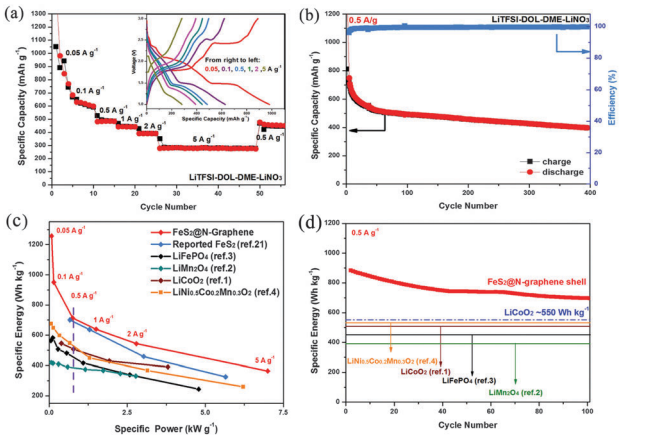

Fig. 4 (a) Rate performances of cells at 0.05, 0.1, 0.5, 1, 2, 5 A g^{-1} (inset is the typical charge–discharge curves), (b) long cycling performance from 2nd to 400th cycle at 0.5 A g^{-1}. (c) Discharge energy density of FeS_2@N-graphene particles compared to other commercial Li-ion cell cathode materials. (d) Discharge energy density of FeS_2@N-graphene particles *vs.* cycle number shown at 0.5 A g^{-1} along with the theoretical discharge specific energy of commercial cathode materials.

reversible reaction of Li_2S. During the charging procedure, theoretically, the iron is oxidized to provide electrons to react with Li_2S to form Li_2FeS_2, then further to form FeS_y. Actually, in the initial stage of Li^+ extraction, iron can react with Li_2S to form Li_2FeS_2 at the interface between the Fe nano-particle and Li_2S (State 1 in Fig. 3c and d) until all the iron and Li_2S transform into Li_2FeS_2 (State 1 to 2.1 in Fig. 3c and d). In this case, smaller particles wrapped in conductive frameworks have shorter Li^+ diffusion distances and more electron transfer channels. This allows reversible redox to proceed with fast kinetics. With the number of extracted Li ions increased, Li_2FeS_2 starts to supply Li ions and electrons to form $Li_{2-x}FeS_2$ (State 2 to 3, in Fig. 3c and d). Note that the intermediate structure of $Li_{2-x}FeS_2$ is unstable and changeable, which directly affects the transfer ability of Li ions. It can be predicted that if the size of the FeS_2 particles becomes smaller and the electronic conductivity of FeS_2 particles gets better, the Li ions and electrons are easier to extract from $Li_{2-x}FeS_2$ due to the shorter Li-ionic diffusion distance and better electronic conductivity. Therefore the shutter reaction due to Li_2S_x ($2 \leq x \leq 8$) and generation of S nano-particles may be avoided because S^{2-} prefers to form $(S_2)^{2-}$ to combine with Fe^{3+} (from State 3.2 to 4 in Fig. 3c and d). S nano-particles are always generated in general cases and have low dissolution ability in electrolytes.[32] Besides shrinking the FeS_2 particle to shorten the Li^+ diffusion distance, $LiNO_3$ plays a very essential role in alleviating parasitic reactions between Li metal and already present sulfur species to optimize cycling the performance of FeS_2 based Li-ion batteries. A mechanism of $LiNO_3$ doping was proposed where $LiNO_3$ can be directly reduced by lithium to Li_xNO_y and oxidized by sulfur species to Li_xSO_y, forming a Li–N–S–O passivating layer coating upon the lithium anodes.[20] In this work, it can be observed that the surface of the Li anode is not smooth with dark species formed on the lithium, *e.g.* the SEM images of lithium anode surfaces after discharging shown in Fig. S9 (ESI†). Additionally, nano-FeS_2@N-graphene cells with two other kinds of electrolytes were investigated and the cycling performances are shown in Fig. S10 (ESI†), further indicating

that the ether-based electrolyte with $LiNO_3$ plays a pivotal role in promoting the electrochemical stability.

The nano-FeS_2@N-graphene for Li-ion cells exhibits good rate capability as shown in Fig. 4a. The reversible specific capacity is also very good with 768, 630, 484, 445, 391 and 285 mA h g^{-1} at 0.05, 0.1, 0.5, 1, 2, 5 A g^{-1} respectively, which is then able to return to 475 mA h g^{-1} at 0.5 A g^{-1} (Fig. 4b). Compared to low conductive PAN matrix encapsulation,[22] FeS_2@N-graphene has a high reversible capacity due to the continuous conductive paths formed by the N-graphene frameworks among the FeS_2 particles. What is more, long-term stability is one of the key challenge for FeS_2 batteries. The Li-ion cells with core–shell FeS_2@N-graphene still have very high capacity (401.7 mA h g^{-1}) after 400 cycles at 0.5 A g^{-1}, corresponding to the specific energy of 637.1 W h kg^{-1} (in Fig. 4b). The coulombic efficiency of any cycle is very close to 100%, which can be attributed to the stable shell structure.

To further clarify reasons behind the good performance of core–shell nano-FeS_2@N-graphene, the AC-impedance measurement was carried out to give curves for the 1st, 5th and 400th cycle in the discharged state (1.2–1.3 V), as shown in Fig. S11 (ESI†). The values of R_{ct} from the 1st to the 5th cycle are changed from 10.5 to 12.2 Ω, and then until the 400th cycle to about 61.4 Ω. Note that these results are much lower than those reported with FeS_2@C materials.[14,15] It is generally believed that the electrical conductivity influences R_{ct} immensely. Hence, the big improvement of values of R_{ct} in this work can be attributed to the N-graphene frameworks being able to provide fast charge transfer channels at the FeS_2/electrolyte interface to reduce the resistance. After long-term cycling, R_{ct} changes little, meaning that the shell structure of nano-FeS_2@N-graphene is very stable.

Furthermore, for evaluating the practical value, we compared specific power-specific energy of core–shell nano-FeS_2@N-graphene to other commercial Li-ion battery cathodes, such as $LiCoO_2$, $LiFePO_4$, $LiMn_2O_4$, $LiNi_{0.5}Co_{0.2}Mn_{0.3}O_2$, *etc.* shown in Fig. 4c and d. The significant advantage of nano-FeS_2@N-graphene is to have very high specific energy at different currents (1275, 950, 713, 639, 543, 364 W h kg^{-1} at 0.05, 0.1, 0.5, 1, 2, 5 A g^{-1} respectively), which are much higher than other commercial Li-ion cell cathodes (Fig. 4c). Even compared to the reported pyrite FeS_2@C,[21] the specific energy of core–shell FeS_2@N-graphene of this work is higher especially at high current rate area, further indicating that uniform and continuous N-graphene carbon frameworks can provide more continuous conductive paths between any prime FeS_2 particles. Fig. 4d shows that the FeS_2@N-graphene has stable cycle specific energy. Compared to the reported $LiCoO_2$ (~504 W h kg^{-1}), $LiNi_{0.5}Co_{0.2}Mn_{0.3}O_2$ (~530 W h kg^{-1} at 0.5 A g^{-1}), $LiFePO_4$ (~450 W h kg^{-1} at 0.5 A g^{-1}) and $LiMn_2O_4$, (~390 W h kg^{-1} at 0.5 A g^{-1}), FeS_2@N-graphene has a higher energy density of 701 W h kg^{-1} after 100 cycles, whose specific energy retention is up to ~80%. Therefore, the FeS_2@N-graphene is a potential Li-ion cathode material for the next generation of Li-ion batteries.

In summary, for solving the problems associated with the electroactive FeS_2 cathode species, a novel core–shell nano-FeS_2@N-graphene was prepared as a novel cathode material for Li-ion batteries. The benefit of the amount of nanosize FeS_2 nano-crystals as the core for Li-ion storage and using coated N-doped graphene as the shell is that core–shell FeS_2@N-graphene exhibits a remarkable specific energy (950 W h kg^{-1} at 0.1 A g^{-1}) and higher specific power (543 W h kg^{-1} at 2.79 kW g^{-1}) than commercial rechargeable LIB cathodes, as well as a stable cycling performance. Hence FeS_2@N-graphene is a very promising candidate as a next generation advanced Li-ion cathode.

The research was financially supported by National Project for EV Batteries (20121110, OptimumNano, Shenzhen), Guangdong Innovation Team Project (No. 2013N080), and Shenzhen Science and Technology Research (Grant No. ZDSY20130331145131323, JCYJ20140903101633318).

Notes and references

1 X. Xiao, X. Liu, L. Wang, H. Zhao, Z. Hu, X. He and Y. Li, *Nano Res.*, 2012, **5**, 395.
2 Y.-L. Ding, J. Xie, G.-S. Cao, T.-J. Zhu, H.-M. Yu and X.-B. Zhao, *Adv. Funct. Mater.*, 2011, **21**, 348.
3 C. Zhu, Y. Yu, L. Gu, K. Weichert and J. Maier, *Angew. Chem., Int. Ed.*, 2011, **50**, 6278.
4 Z. Wu, S. Ji, J. Zheng, Z. Hu, S. Xiao, Y. Wei, Z. Zhuo, Y. Lin, W. Yang, K. Xu, K. Amine and F. Pan, *Nano Lett.*, 2015, **15**, 5590.
5 T. A. Yersak, H. A. Macpherson, S. C. Kim, V.-D. Le, C. S. Kang, S.-B. Son, Y.-H. Kim, J. E. Trevey, K. H. Oh, C. Stoldt and S.-H. Lee, *Adv. Energy Mater.*, 2013, **3**, 120.
6 P. J. Masset and R. A. Guidotti, *J. Power Sources*, 2008, **177**, 595.
7 D. Yichen, Z. Xiaoshu, Z. Xiaosi, H. Lingyun, D. Zhihui and B. Jianchun, *J. Mater. Chem. A*, 2015, **3**, 6787.
8 D. Yichen, Z. Xiaoshu, S. Ling, L. Yafei, Z. Xiaosi and B. Jianchun, *J. Phys. Chem. C*, 2015, **119**, 15874.
9 J. Cabana, L. Monconduit, D. Larcher and M. R. Palacin, *Adv. Mater.*, 2010, **22**, E170.
10 S. S. Zhang, *J. Mater. Chem. A*, 2015, **3**, 7689.
11 H. Xue, D. Y. W. Yu, J. Qing, X. Yang, J. Xu, Z. Li, M. Sun, W. Kang, Y. Tang and C.-S. Lee, *J. Mater. Chem. A*, 2015, **3**, 7945.
12 F. Rosamaria, J. R. Dahn and C. H. W. Jones, *J. Electrochem. Soc.*, 1989, **136**, 3206.
13 A. Le Mehaute and A. Dugast, *J. Power Sources*, 1983, **9**, 359.
14 D. Zhang, Y. J. Mai, J. Y. Xiang, X. H. Xia, Y. Q. Qiao and J. P. Tu, *J. Power Sources*, 2012, **217**, 229.
15 L. Liu, Z. Yuan, C. Qiu and J. Liu, *Solid State Ionics*, 2013, **241**, 25.
16 L. Li, M. Caban-Acevedo, S. N. Girard and S. Jin, *Nanoscale*, 2014, **6**, 2112.
17 V. Pelé, F. Flamary, L. Bourgeois, B. Pecquenard and F. Le Cras, *Electrochem. Commun.*, 2015, **51**, 81.
18 T. Evans, D. M. Piper, S. C. Kim, S. S. Han, V. Bhat, K. H. Oh and S. H. Lee, *Adv. Mater.*, 2014, **26**, 7386.
19 E. Strauss, *J. Power Sources*, 2003, **115**, 323.
20 A. Manthiram, Y. Fu, S. H. Chung, C. Zu and Y. S. Su, *Chem. Rev.*, 2014, **114**, 11751.
21 J. Liu, Y. Wen, Y. Wang, P. A. van Aken, J. Maier and Y. Yu, *Adv. Mater.*, 2014, **26**, 6025.
22 S.-B. Son, T. A. Yersak, D. M. Piper, S. C. Kim, C. S. Kang, J. S. Cho, S.-S. Suh, Y.-U. Kim, K. H. Oh and S.-H. Lee, *Adv. Energy Mater.*, 2014, **4**, 1300961.
23 A. L. Reddy, A. Srivastava, S. R. Gowda, H. Gullapalli, M. Dubey and P. M. Ajayan, *ACS Nano*, 2010, **4**, 6337.
24 Z. S. Wu, W. Ren, L. Xu, F. Li and H. M. Cheng, *ACS Nano*, 2011, **5**, 5463.
25 N. Mahmood, C. Zhang, F. Liu, J. Zhu and Y. Hou, *ACS Nano*, 2013, **7**, 10307.
26 J. Hu, J. Zheng, L. Tian, Y. Duan, L. Lin, S. Cui, H. Peng, T. Liu, H. Guo, X. Wang and F. Pan, *Chem. Commun.*, 2015, **51**, 7855.
27 Y. Wang, H. Sun, X. Duan, H. M. Ang, M. O. Tadé and S. Wang, *Appl. Catal., B*, 2015, **172–173**, 73.
28 W. Yang, X. Liu, X. Yue, J. Jia and S. Guo, *J. Am. Chem. Soc.*, 2015, **137**, 1436.
29 S. Zhen, S. Lin, C. Jing, B. Wen, W. Feng and X. Xing, *ACS Nano*, 2011, **5**, 4350.
30 Y. Zhang, W. J. Jiang, L. Guo, X. Zhang, J. S. Hu, Z. Wei and L. J. Wan, *ACS Appl. Mater. Interfaces*, 2015, **7**, 11508.
31 S. Zhang, *J. Electrochem. Soc.*, 2012, **159**, A920.
32 C. Hongwei, W. Changhong, D. Weiling, L. Wei, D. Zhaolong and C. Liwei, *Nano Lett.*, 2015, **15**, 798.

